

# Using Wavelet Domain Fingerprints to Improve Source Camera Identification

Xinle Tian<sup>a</sup>, Matthew A. Nunes<sup>a,\*</sup>, Emiko Dupont<sup>a</sup>, Shaunagh Downing<sup>b</sup>,  
Freddie Lichtenstein<sup>b</sup>, Matt Burns<sup>b</sup>

<sup>a</sup>*Department of Mathematical Sciences, University of Bath, Claverton Down, BA2  
7AY, Bath, United Kingdom*

<sup>b</sup>*CameraForensics, Bristol, BS1 6AA, United Kingdom*

---

## Abstract

Camera fingerprint detection plays a crucial role in source identification and image forensics, with wavelet denoising approaches proving to be particularly effective in extracting sensor pattern noise (SPN). In this article, we propose a modification to wavelet-based SPN extraction. Rather than constructing the fingerprint as an image, we introduce the notion of a wavelet domain fingerprint. This avoids the final inversion step of the denoising algorithm and allows fingerprint comparisons to be made directly in the wavelet domain. As such, our modification streamlines the extraction and comparison process. Experimental results on real-world datasets demonstrate that our method not only achieves higher detection accuracy but can also significantly improve processing speed.

*Keywords:* Sensor Pattern Noise, Source Camera Identification, Discrete Wavelet Transform, Sensor Fingerprint, Signal Processing

---

## 1. Introduction

Camera fingerprint detection is a fundamental technique in digital image forensics, which focuses on determining the source and authenticity of images while detecting any manipulations applied to them [37]. The analysis of digital images or videos can serve as scientific evidence in legal cases involving surveillance, cybercrime, and other forensic investigations, for example, to combat film piracy or fake news generation. One key area of digital image forensics is source camera identification (SCI), which seeks to determine the specific camera used to capture an image. This plays a crucial role in forensic inquiries, aiding in the verification of image origins and supporting legal proceedings [17, 36].

---

\*Corresponding author

*Email addresses:* xt373@bath.ac.uk (Xinle Tian), man54@bath.ac.uk (Matthew A. Nunes), eahd20@bath.ac.uk (Emiko Dupont), shaunagh@cameraforensics.com (Shaunagh Downing), fred@cameraforensics.com (Freddie Lichtenstein), matt@cameraforensics.com (Matt Burns)

Common methods for source camera identification rely on various image characteristics, including lens aberration [12], sensor noise patterns [29], chromatic aberration [40], CFA interpolation [7, 9, 10], as well as classification models based on features extracted from images using classical statistical measures [26] or more recently automatically via deep learning (see e.g. [23, 42, 16, 30]). With advancements in digital forensics, researchers have established that each camera produces a unique fingerprint within its images, commonly known as sensor pattern noise (SPN), which is dominated by Photo-Response Non-Uniformity (PRNU) [31, 6]. There has been a growing literature on PRNU-based device identification, see e.g. [29, 21, 22, 1]. This method of source identification is considered highly reliable [25, 18], as PRNU arises from manufacturing imperfections in camera sensors, making it distinct for each model [3]. For overviews of PRNU extraction methods, we refer the reader to [28, 2].

In many scientific applications, such as cybercrime, practitioners are faced with the challenging scenario in which they have a potentially suspect candidate image and it is of interest to compare this image to all entries of a large image database to determine possible camera matches. In this setting, it is rare to have sufficient copies from the same camera with which to train a full classification model, precluding the use of deep learning for camera identification, and thus an unsupervised approach is needed; see also [22] for additional insight on the need for large-scale testing in digital forensics. Due to the typically large number of image comparisons to be undertaken, it is of the utmost importance that the image processing involved in such comparisons is computationally efficient. In this article, we particularly focus therefore on the situation in which a raft of PRNU-based image tests is to be performed.

Among PRNU-based camera source identification methods, frequency domain denoising approaches, using Fourier and wavelet transforms, have gained attention for their effectiveness in isolating high frequency noise components (believed to contain the camera sensor pattern noise) from structured image content, see e.g. [29, 11, 4, 45]. In this process, a sensor pattern fingerprint is extracted from each image using a combination of image transforms and frequency domain filtering. These components are often subsequently processed or additionally filtered in the image domain to remove unwanted artifacts before comparison, see e.g. [11, 20, 2].

In this article, we propose a general approach to modify current state-of-the-art frequency-based fingerprint extraction and processing to improve computational efficiency of PRNU-based image comparison and/or testing accuracy. More specifically, we advocate judicious fingerprint comparison directly in the wavelet domain, rather than the current approach of performing comparisons on the extracted PRNU components in the original image domain. Our reasoning behind the proposed modifications stems from the fact that the Fourier/wavelet transforms used are orthonormal. This means that, for the purposes of the comparisons, the information contained in the (filtered) frequency domain coefficients is the same as that in the image domain, effectively rendering inversion back to the image domain unnecessary. This insight enables us to streamline the extraction pipeline by avoiding fingerprint reconstruction and thus reducing

computational cost. This provides particular benefit in the large-scale testing applications described above. Note that our intention with this work is not to propose new denoising filters; as such we explore the proposed wavelet domain fingerprint comparison with commonly used existing wavelet filtering methods.

The rest of the article is organised as follows. Section 2 provides a brief overview of wavelet transforms and details common denoising filters used in PRNU extraction. Our proposed approach to modify these denoising filters is introduced in Section 3, with experiments demonstrating the pipeline in Section 4. Section 5 concludes and provides a discussion of the contribution of this article.

## 2. Background

### 2.1. Discrete wavelet decompositions in image denoising

Prior research has posited that images captured by a camera can be conceptualised as a combination of the "true scene" of an image, coupled with a camera fingerprint and additional noise [11]. Typically, the representation of the actual scene is retained within the low frequency components of the image data, whereas the noise/fingerprint is contained in the higher frequency components. This motivates the use of wavelet transforms, a natural tool for decomposing images into different frequency components.

A wavelet transform represents an input image as a linear combination of information in different directions and at different frequencies (known as wavelet scales or levels) up to a given level  $J$ , known as the primary resolution level. In practice, the coefficients of the transform are obtained from successive applications of low-pass and high-pass filters on the rows and columns of the image, resulting in direction-specific coefficients for the horizontal, vertical and diagonal features at each level. Starting from the finest resolution of the image, the low-pass filter produces 'approximation' or 'scaling' coefficients corresponding to a coarser representation of the image, while the high-pass filter outputs 'detail' coefficients representing the details lost in this approximation. The detail coefficients obtained through this process together with the approximation coefficients at the coarsest resolution  $J$  form a pyramid structure in which the total number of coefficients equals the image size. The transformation from the image domain to these coefficients in the wavelet (frequency) domain is an invertible linear transformation, referred to as the discrete wavelet transform (DWT).

The output of the DWT is often visually presented as a subdivision of the original image domain into a collection of smaller subimages, each of which illustrate different components of the transform. More specifically, the approximation coefficients (labelled  $cA$ ) correspond to a subimage capturing the lowest resolution features of the original image such as the background scene or mean signal, while for each level of the transform, the detail coefficients (denoted  $cH$ ,  $cV$ ,  $cD$  for the horizontal, vertical and diagonal directions, respectively) lead to three subimages showing the details that would be added in each direction if the resolution of the image approximation was increased by one level. An illustration of this process can be seen in Figure 1.

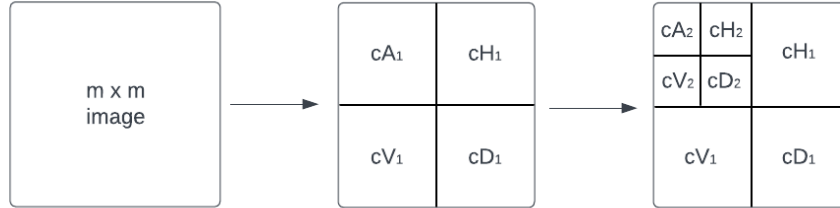


Figure 1: Illustration of DWT applied to an image with level  $J = 2$ .

In image denoising, the DWT is combined with thresholding or shrinking of the finer scale detail coefficients in the wavelet domain. This will suppress the high frequency components of the image data most likely to be noise, while keeping the remaining features of the image intact. The denoised image is then reconstructed from the modified coefficients using the inverse DWT. For comprehensive overviews of wavelet transforms and denoising, we refer the reader to [34, 41, 39].

The SPN is often seen as the residual between the noise-suppressed image and the random background noise; this can be obtained either through retaining certain high frequency components in the wavelet domain before inversion [11] or by computing the residual image in the original data domain [45]. However, SPN extraction is challenging as the unstructured high frequency behaviour of the SPN makes it difficult to distinguish it from random noise in the image. Whilst classical wavelet thresholding and coefficient shrinkage methods are well-established in the statistical literature for signal denoising, they do not perform well in the SPN setting. This has led researchers to explore spatially-adaptive denoising, such as estimating the noise field across the image to inform filtering methods, such as Wiener filtering, see e.g. [32]. In addition, other wavelet transforms have been used recently to improve spatial or directional information used in the denoising, at the expense of possible increased computational cost, such as undecimated wavelet transforms [5], or the dual tree complex wavelet transform (DTCWT) [45].

## 2.2. Existing PRNU denoising methodology

In this section, we provide details on the main two PRNU extraction methods used later in the article, which we modify to demonstrate and evaluate our proposed wavelet-domain fingerprint methodology. More specifically, we describe 1) the *Locally Adaptive Window-based denoising* (LAW) method that has been proposed by [33] and further studied in the PRNU context by [29, 11, 24], as well as 2) the denoising approach based on the dual tree complex wavelet transform of [45]. We focus on these two wavelet filtering methods since the LAW method is one of the most commonly-used in the literature, and the method of [45] has been shown to outperform other state-of-the-art PRNU extraction

methods such as the recently proposed BM3D filtering technique [14], known also to be computationally intensive to run.

### 2.2.1. Locally Adaptive Window-based denoising (Mihcak's filter)

The algorithm proposed in [29] is a wavelet-based denoising method that uses local statistical modelling of wavelet coefficients. The spatially-adaptive filters used in this SPN workflow is referred to as *Mihcak's filter* in some previous studies [4]. The proposed SPN extraction method begins by applying the DWT to the noisy image ( $I_{m \times m}$ ), decomposing it into subimages at multiple scales and orientations. Since the coefficients in each subimage are naturally spatially arranged due to being (smaller) filtered versions of the original image, instead of using a global threshold for coefficient shrinkage, the method estimates the local mean and variance of high frequency wavelet coefficients within small neighbourhoods, assuming a local Gaussian distribution. Specifically, for each coefficient  $w(k_1, k_2)$ , the local variance is estimated using a neighbourhood window  $\mathcal{N}(k_1, k_2)$  around the coefficient:

$$\hat{\sigma}_N^2(k_1, k_2) = \max \left( 0, \frac{1}{N} \sum_{(i_1, i_2) \in \mathcal{N}(k_1, k_2)} w^2(i_1, i_2) - \sigma_n^2 \right),$$

where  $N$  is the number of coefficients in the local window, and  $\sigma_n^2$  is the estimated noise variance. This neighbourhood approach to thresholding is possible due to being able to arrange the decomposition coefficients spatially. The subtraction of  $\sigma_n^2$  ensures that only the true local variance of the signal is retained. The application of the maximum function prevents negative variance estimates, which could otherwise occur in regions dominated by noise. In practice,  $\hat{\sigma}_N^2(k_1, k_2)$  is computed for a range of local windows, for example with  $N = 3^2, 5^2, 7^2, 9^2$ , and for each pixel, the final estimate  $\hat{\sigma}^2(k_1, k_2)$  is taken to be the minimum of those computed (see e.g.[33, 32, 29]).

Once the local variance is estimated, an *adaptive local Wiener-like shrinkage* is applied to attenuate noise while preserving significant image structures. The denoised coefficient is computed as:

$$\hat{w}(k_1, k_2) = \frac{\hat{\sigma}^2(k_1, k_2)}{\hat{\sigma}^2(k_1, k_2) + \sigma_n^2} w(k_1, k_2). \quad (1)$$

This equation scales each coefficient based on the ratio of its local signal variance to the total variance (signal + noise). When the local variance  $\hat{\sigma}^2(k_1, k_2)$  is much larger than the noise variance  $\sigma_n^2$ , the shrinkage factor approaches 1, meaning the coefficient remains largely unchanged. However, when the local variance is close to the noise variance, the shrinkage factor becomes small, reducing the coefficient's magnitude to suppress noise. This adaptive process ensures that edges and textures in the image are preserved while noise is attenuated more aggressively in smooth areas, leading to effective denoising without excessive blurring.

The filtered coefficients after the shrinkage are then transformed back to the image domain using the inverse wavelet transform (IDWT) to reconstruct the filtered image ( $\tilde{I}_{m \times m}$ ). For colour (multi-channel) images, this procedure is done to each image channel, and the resulting channels are often combined using a luminance-based grayscaleing using the linear combination of the R, G, B channels (see e.g. [21, 2]):

$$\tilde{I}_{m \times m} = 0.299\tilde{I}_{m \times m}^R + 0.587\tilde{I}_{m \times m}^G + 0.114\tilde{I}_{m \times m}^B.$$

*Denoised image post-processing.* In PRNU applications, the resulting denoised images  $\tilde{I}_{m \times m}$  may still contain geometric artifacts caused by the sensor design, which it is recommended to remove prior to comparison [11]; these artifacts are sometimes referred to as *shared components* [2]. Typically, this artifact removal consists of two steps. Firstly, row- and columnwise means are subtracted from the denoised image; this *zero-mean* operation helps in removing linear patterns found in lower quality cameras [11]. A final *Wiener-type filtering* step is performed in the Fourier domain, to further refine the PRNU estimate by suppressing any residual polygonal structures in the image. This is achieved by computing the 2D Discrete Fourier Transform (DFT) to transform the image  $\tilde{I}_{m \times m}$  is transformed into the frequency domain:

$$F(\omega_1, \omega_2) = \mathcal{F}\{\tilde{I}_{m \times m}\}(\omega_1, \omega_2), \quad (2)$$

where  $F(\omega_1, \omega_2)$  represents the Fourier frequency coefficients of the noisy image. Adaptive Wiener filtering is then applied to the Fourier coefficients, where the Wiener filter estimates the power spectrum of the noise and applies a signal-dependent attenuation:

$$\hat{F}(\omega_1, \omega_2) = F(\omega_1, \omega_2) \cdot \frac{\hat{S}(\omega_1, \omega_2)}{\hat{S}(\omega_1, \omega_2) + S_n}, \quad (3)$$

where  $\hat{S}(\omega_1, \omega_2)$  is the estimated local power spectrum of the image  $\tilde{I}_{m \times m}$ , computed using the same method as described in Equation (2.2.1) and  $S_n$  is the estimated power spectrum of the noise. Lastly the filtered Fourier coefficients are converted back into the image domain using the inverse DFT (IDFT):

$$f(k_1, k_2) = \mathcal{F}^{-1}\{\hat{F}\}(\omega_1, \omega_2). \quad (4)$$

This results in a denoised fingerprint  $f_{m \times m}$  where remaining noise distortions have been adaptively suppressed. A detailed algorithm for LAW is presented in the pseudocode in Algorithm 1 for the general case of coloured images. Figure 2 illustrates the LAW method process for extracting camera fingerprints using an image from an open data source [19], which can be accessed from <https://www.kaggle.com/datasets/micscodes/dresden-image-database>.

### 2.2.2. Dual tree complex wavelet transform PRNU extraction

The (2D) dual tree complex wavelet transform was introduced by [27] as a tool to extract improved spatial and directional information from images

---

**Algorithm 1:** The LAW SPN fingerprint extraction algorithm for colour images

---

**Input** : Image  $I_{m \times m}$

**Output:** SPN fingerprint  $f_{m \times m}$

**STEP 1:** Load image  $I_{m \times m}$

**STEP 2:** Perform wavelet domain filtering:

**for** each image channel  $i \in \{R, G, B\}$  **do**

1. Perform DWT with primary resolution level  $J$

2. **for** each wavelet level  $j = 1, \dots, J$  **do**

Apply locally adaptive Mihcak filter to high frequency coefficients  $cH, cV, cD$

**end**

3. Set the approximation coefficients  $cA$  to zero

4. Perform IDWT using zeroed  $cA$  and filtered coefficients  $cH, cV, cD$  to get filtered image channel  $\tilde{I}_{m \times m}^i$

**STEP 3:** Perform grayscaling to combine filtered image channels

**STEP 4:** Apply Wiener filtering in Fourier domain:

1. Perform DFT to obtain frequency components  $F(\omega_1, \omega_2)$

2. Apply locally adaptive Mihcak filter to obtain filtered frequency components  $\hat{F}(\omega_1, \omega_2)$

3. Perform IDFT to get final image domain fingerprint  $f_{m \times m}$

---

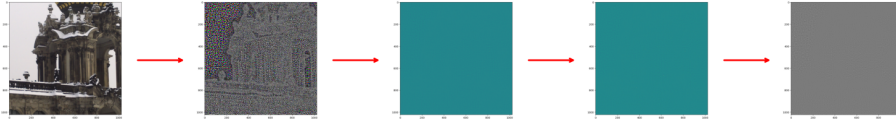


Figure 2: Illustration of the LAW method applied to an image. The PRNU extraction image processing pipeline consists of (i) wavelet decomposition with spatially adaptive filtering and inversion (ii) grayscaling of denoised colour images (iii) zero-mean normalisation and (iv) second Wiener filtering to extract the fingerprint.

compared to the standard DWT. The DTCWT consists of two sets of filters which operate on the components of an image to form complex-valued wavelet coefficients. Due to the two filterbanks, at each level of the transform, the three directional coefficient subimages ( $cH, cD, cV$ ) of the DWT are replaced

by six subimages ( $cH^1, cV^1, cD^1, cH^2, cV^2, cD^2$ ) – three for each branch of the tree [38]. [45] introduced an SPN extraction method based on the DTCWT which was shown to perform well in SPN applications, especially when edges are present in images.

The SPN extraction method proposed in [45] has a similar form to a traditional decomposition-threshold-inversion denoising method, except that due to the SPN application, interest lies in retaining the noise from the denoiser as a residual image, rather than the denoised image itself. More specifically, the method firstly performs the DTCWT with a chosen primary resolution level, subsequently thresholding the six wavelet coefficient subimages by applying the local spatially adaptive filtering of [33, 32] on the (*complex*) *magnitude* of the coefficients. The inverse DTWCT (IDTCWT) is then performed on the resulting coefficient pyramid to produce a denoised image; the SPN is computed as the residual of the denoised image from the original image. An overview of the DTCWT SPN extraction method is in Algorithm 2.

---

**Algorithm 2:** The DTCWT-based SPN fingerprint extraction algorithm for colour images

---

**Input** : Image  $I_{m \times m}$

**Output:** SPN fingerprint  $f_{m \times m}$

**STEP 1:** Load image  $I_{m \times m}$

**STEP 2:** Perform wavelet domain filtering:

**for** each image channel  $i \in \{R, G, B\}$  **do**

1. Perform DTCWT with primary resolution level  $J$

2. **for** each wavelet level  $j = 1, \dots, J$  **do**

Apply locally adaptive Mihcak filter to high frequency coefficients  $cH^1, cV^1, cD^1, cH^2, cV^2, cD^2$

**end**

3. Perform IDTCWT using filtered high frequency coefficients  $cH^1, cV^1, cD^1, cH^2, cV^2, cD^2$  and approximation coefficients  $cA$  to get filtered

image channel  $\hat{I}_{m \times m}^i$

4. Form channel-specific SPN image by computing residual from original image channel:  $\tilde{I}_{m \times m}^i = I_{m \times m}^i - \hat{I}_{m \times m}^i$

**STEP 3:** Perform grayscaleing to combine filtered colour image

channels and get final image domain fingerprint  $f_{m \times m}$

---

The approach of [45] does not discuss including shared component removal as employed by [29, 11] for the DWT-based SPN extraction method (see Section 2.2.1); for the tampering localization application the authors considered,

this may not have been necessary or beneficial. However, we discuss possible inclusion of this aspect of fingerprint extraction in Section 4.

### 2.3. Criteria for source identification

Establishing criteria to determine whether images originate from the same device is crucial for making accurate final decisions. This step is significant, as it can directly impact the outcomes of the classification process. However, it is also a flexible component that ultimately depends on the analyst’s decisions and specific application context.

In our study, we applied the simple cosine similarity test for its efficiency in measuring the angular distance between feature vectors, making it a widely used metric for data comparisons. For a pair of feature vectors  $f_1$  and  $f_2$  (representing extracted fingerprints from two images) their cosine similarity is given by:

$$\frac{f_1 \cdot f_2}{\|f_1\| \|f_2\|} \quad (5)$$

where  $f_1 \cdot f_2$  is the dot product of the vectors, and  $\|f_1\|$  and  $\|f_2\|$  are their respective Euclidean norms. This measure provides a normalized similarity score between -1 and 1, where a higher value indicates greater similarity between the vectors.

After we obtain the cosine similarity score for each image pair, we need a threshold,  $\lambda$ , to determine whether the two images originate from the same source. If the similarity score falls below this threshold, the images are classified as coming from different sources; otherwise, they are considered to be from the same source.

A simple and effective method to determine this threshold can be derived from Receiver Operating Characteristic (ROC) curve analysis, a graphical representation used to evaluate the performance of a binary classification model. The ROC curve illustrates the trade-off between the true positive rate (TPR) and the false positive rate (FPR) at various benchmark value settings of a parameter. The TPR measures the proportion of actual positives correctly identified by the method, while the FPR quantifies the proportion of actual negatives that are incorrectly classified as positives. In our case, we consider the ROC curve obtained by varying the value of  $\lambda$ .

#### Threshold 1

For a given ROC curve, Youden’s Index [43] is the maximum difference between the TPR and the FPR. This difference should ideally be large, so a natural way to identify the optimal value for  $\lambda$  is given by

$$\lambda_{YI} = \operatorname{argmax}_{\lambda} (\operatorname{TPR}(\lambda) - \operatorname{FPR}(\lambda)).$$

This method helps in selecting a threshold that provides the best trade-off between correctly identifying same-source images while minimizing misclassification errors. The downside is that it may give multiple potential values, making

it challenging to select the most appropriate one. Careful evaluation and validation is needed in order to choose the value that best balances sensitivity and specificity. In general, from an application perspective, it is advisable to choose the value that yields the highest TPR.

### *Threshold 2*

An alternative approach for setting the classification criterion is to control the true negative rate (TNR) (the proportion of actual positives correctly identified by the method) which should ideally be large. More specifically, if our desired value for TNR is  $R$ , then since  $\text{TNR}(\lambda) = 1 - \text{TPR}(\lambda)$ , the chosen threshold is the value of  $\lambda$  for which  $\text{TPR}(\lambda) = 1 - R$ .

This method minimises the risk of mistakenly classifying images as being from the same source when they are not, while still achieving good chances of correctly identifying images that do originate from the same source. This approach aligns with scientists’ objectives and practical operational needs, where minimising false positives is critical for maintaining the integrity and reliability of forensic decisions.

In the applications in Section 4, we will present results that include both the criterion values and their corresponding TPR and TNR.

## **3. Proposed methodology**

In this section, we present our proposed approach to fingerprint identification, which streamlines wavelet-based extraction pipelines by removing unnecessary processing steps. In many cases, accuracy and/or computational efficiency of comparisons can be gained by performing comparisons directly in the wavelet domain.

Since the wavelet transformation is a linear operator based on an orthonormal wavelet basis, Parseval’s theorem states that the signal energy is preserved when performing the transform (or equivalently its inverse), see e.g. [13]. Moreover, the cosine similarity measure used for comparisons is invariant under orthonormal transformations. Motivated by this, we hypothesise that, not only do the essential properties of the SPN image remain the same before and after performing the inverse wavelet transform, but the key information useful to SPN comparison is more effectively harnessed from the wavelet coefficients. In effect, this defines a new notion of camera fingerprint, namely a representation of the SPN in the wavelet domain, that we refer to as the WD fingerprint.

Building on this idea, we propose modifications to both of the wavelet-based PRNU extraction methods outlined in Section 2.2.

### *3.1. Proposed single channel wavelet domain fingerprint extraction with the DWT*

In this section, we propose a modified version of the original LAW method outlined in Section 2.2.1, which we refer to as *Wavelet Domain Locally Adaptive Window-based denoising* (WDLAW). Instead of constructing an SPN fingerprint

in the image domain, WDLAW defines a fingerprint directly in the wavelet domain where the SPN information corresponds to the vector of detail coefficients ( $cH, cV, cD$ ) from the DWT decomposition. This reduces the dimension of the fingerprint, decreasing computational overhead at the comparison stage of analysis.

The size of the WD fingerprint in this case can be computed as

$$l = \sum_{j=1}^J \frac{3}{4} \times \left( \frac{m}{2^{j-1}} \times \frac{m}{2^{j-1}} \right) = \frac{3}{4} m^2 \sum_{j=1}^J (2^{-J+1})^2, \quad (6)$$

where  $J$  is the primary resolution level of the DWT. For any choice of  $J, l < m^2$ , and for small  $J, l$  approximates to  $\frac{3}{4}m^2$ . In other words, the number of pixels used for the wavelet domain fingerprints is always less than the total number of pixels of the image, and for small  $J$ , only about 75% of the pixels, compared to the full  $m^2$  for the LAW method. Note that since we are only using the wavelet coefficients in the fingerprint, we do not need to perform the zeroing of the approximation coefficients  $cA$  in STEP 2-3) of Algorithm 1.

Another step reconsidered for efficiency purposes in our proposed techniques is the row-/columnwise zero mean operation to suppress regular grid artifacts before applying the final Wiener-type filter. In our experience, this zero mean operation has a minor effect compared to that of the Wiener filter when performing fingerprint comparison, thus we do not perform zero mean filtering; it may however, be of more importance in other settings where the fidelity of the fingerprint is the focus. Indeed, our analysis using the chosen metrics described above shows that this step does not impact the final results.

An algorithmic description of WDLAW is shown in Algorithm 3. Note that due to the removal of the zero mean filtering and wavelet inversion steps, our proposed technique essentially performs Fourier domain filtering as described in (2)-(4) immediately in the wavelet domain. Such back-to-back nonlinear filtering has been used to good effect in other settings, see e.g. [35]. Figure 3 illustrates the WDLAW method for a single level wavelet decomposition for clarity. Note that in all figures, wavelet coefficients have been normalised for improved visualisation.

### 3.2. Proposed RGB image wavelet domain fingerprint extraction with the DWT

We now explore wavelet domain fingerprint extraction for RGB images.

As mentioned in Section 2.2, for colour images grayscaleing is usually performed after wavelet filtering and inversion in the PRNU processing pipeline (STEP 3 in both Algorithm 1 and Algorithm 2). As noted in [2], this grayscaleing operation can instead be performed prior to analysis, so that the SPN extraction can be performed on a single ‘luminance’ channel. The motivation for the first approach stems from per-channel wavelet decompositions potentially providing more nuanced information on the channelwise SPN fingerprint (at the cost of three DWT computations), however this extra information is potentially subsequently ‘lost’ when performing the grayscaleing prior to artifact removal. On the

---

**Algorithm 3:** The single channel WDLAW fingerprint extraction algorithm

---

**Input** : Image  $I_{m \times m}$

**Output:** WD fingerprint  $f_l$

**STEP 1:** Load image  $I_{m \times m}$

**STEP 2:** Perform frequency domain filtering:

1. Perform DWT with primary resolution level  $J$
2. **for** each wavelet level  $j = 1, \dots, J$  **do**
  - (a) Apply locally adaptive Mihcak’s filter to high frequency coefficients  $cH, cV, cD$
  - (b) Apply Wiener filtering in Fourier domain:
 **for** coefficient subimages  $cH, cV, cD$  **do**
    - i. Perform DFT to obtain frequency components  $F(\omega_1, \omega_2)$
    - ii. Apply locally adaptive Mihcak filter to obtain filtered frequency components  $\hat{F}(\omega_1, \omega_2)$
    - iii. Perform IDFT to get artifact-free wavelet coefficients

**STEP 3:** Concatenate wavelet coefficients into fingerprint  $f_l$

---

other hand, performing grayscaling first, whilst computationally more efficient, does not retain possibly useful colour information from the outset of the extraction. The grayscaling operation will contribute to the computational cost of fingerprint extraction, but potentially speed up comparison of fingerprints. An alternative is to keep all channels in the fingerprint, i.e. perform no grayscaling, at the cost of a more computationally expensive fingerprint comparison.

Our proposal for wavelet domain fingerprint extraction of colour images is to adopt a ‘grayscale first’ approach, which we term gray-WDLAW. In other words, this procedure begins by converting the input image to grayscale and then proceeds as in the single channel technique described in Algorithm 3. However, in the experimental evaluation in Section 4, we also consider two other variants of our WDLAW technique for colour images (a) rgb-WDLAW, in which no grayscaling is performed, i.e. the fingerprint consists of wavelet coefficients from each direction and channel (of size  $3l$ , where  $l$  is given by (6)), and (b) WDLAW-gray, in which grayscaling is performed in the wavelet domain after the back-to-back wavelet and Fourier domain filtering.

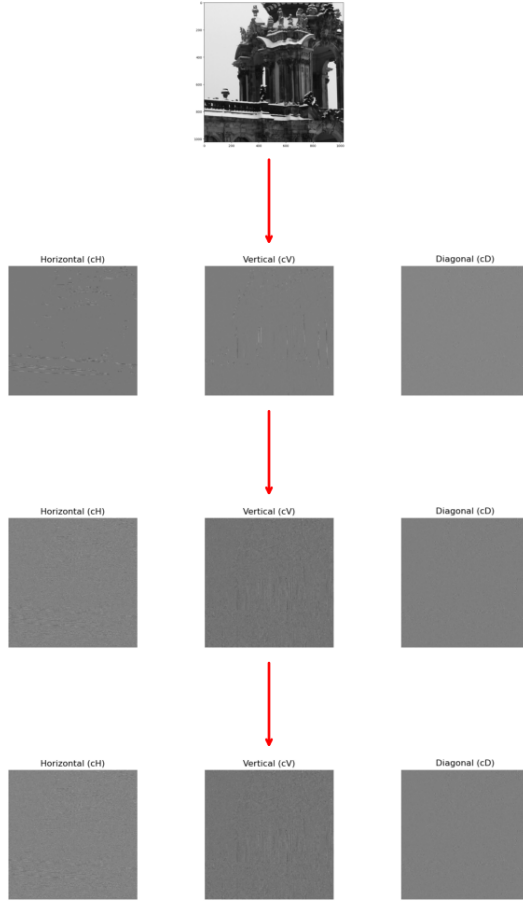


Figure 3: Illustration of the WDLAW method applied to the grayscale image from Figure 2, including (i) applying the DWT to obtain the high frequency coefficients  $cH$ ,  $cV$  and  $cD$  (ii) applying spatially adaptive filtering to these coefficients in the wavelet domain (iii) applying second Wiener filtering in the wavelet domain. The WD fingerprint is obtained by concatenating the resulting coefficients into a vector  $f_l$ .

### 3.3. Proposed wavelet domain fingerprint extraction with the DTCWT

Given that SPN fingerprint extraction with the DTCWT in [45] is a relatively recent development, our interest also lies in testing whether a wavelet domain approach could be extended to use alternative wavelet decompositions beyond the traditional DWT. To this end, we consider several modifications to the extraction method of [45]. Firstly, motivated by the LAW method, we introduce the LAW-DTCWT algorithm as our base extraction method, which employs the DTCWT at the decomposition and inversion stages in STEP 2 of Algorithm 1 instead of the DWT. This differs from the ‘residual image’ extraction approach of [45], since it essentially performs low-pass filtering to remove mean structure

in STEP 2-3) via setting approximation coefficients to zero; this could be viewed as a hybrid between the LAW method of [29, 11] and that of [45]. Secondly, we propose a wavelet domain version of the LAW-DTCWT base technique. More specifically, we perform the same modifications that we considered for the WDLAW method (grayscale first, no wavelet inversion, no zero-mean operation), to form a wavelet domain fingerprint extraction method for RGB images, which we call gray-WDLAW-DTCWT. The detailed steps for applying our proposed wavelet domain approach are outlined in Algorithm 4 below.

---

**Algorithm 4:** The gray-WDLAW-DTCWT fingerprint extraction algorithm for RGB images

---

**Input** : RGB Image  $I_{m \times m}$

**Output:** WD fingerprint  $f_{4l}$

**STEP 1:** Load RGB Image  $I_{m \times m}$

**STEP 2:** Perform grayscale on  $I_{m \times m}$

**STEP 3:** Perform frequency domain filtering:

1. Perform DTCWT with primary resolution level  $J$

2. **for** each wavelet level  $j = 1, \dots, J$  **do**

(a) Apply locally adaptive Mihcak's filter to high frequency coefficients  $cH^1, cV^1, cD^1, cH^2, cV^2, cD^2$

(b) Apply Wiener filtering in Fourier domain:

**for** coefficient subimages  $cH^1, cV^1, cD^1, cH^2, cV^2, cD^2$  **do**

i. Perform DFT to obtain frequency components  $F(\omega_1, \omega_2)$

ii. Apply locally adaptive Mihcak filter to obtain filtered frequency components  $\hat{F}(\omega_1, \omega_2)$

iii. Perform IDFT to get artifact-free wavelet coefficients

**STEP 4:** Concatenate wavelet coefficients into fingerprint  $f_{4l}$

---

Recall that for the DTCWT, the wavelet coefficients are complex-valued and hence are filtered according to their complex magnitude. After the initial Mihcak filter, the resulting coefficients will still be complex-valued, and thus our wavelet domain approach means that the second Wiener filter needs to be modified for use on complex-valued coefficients. We do this in a similar way to the first filtering, i.e. using the complex magnitude of the filtered coefficients. Note that the resulting fingerprint from Algorithm 4 will consist of six complex-valued subimages of coefficients before concatenation. To perform fingerprint comparison with measures such as the cosine similarity (5), these coefficients need to be embedded into the real Euclidean space prior to computation of the

metric. In effect, due to (6) this means that the fingerprints are vectors of size  $4l$  ( $2l$  coefficients, each of which has a real and an imaginary part). This means that this approach requires more in terms of fingerprint storage and computational cost for fingerprint comparison compared with the WDLAW method, but may be beneficial in accuracy due to improved directional information [27, 38, 45].

#### 4. Evaluation of proposed PRNU extraction techniques

In this section, we describe the experiments undertaken to evaluate our proposed wavelet domain fingerprint extraction methods.

##### 4.1. Experimental setup

Our experiments were performed using RGB images from the open-source *Dresden Image Database* [19]. For our analysis, we selected a subset of the dataset consisting of original JPG images from 26 different camera devices, with each device contributing 5 images. Each image was centre-cropped to a resolution of  $1024 \times 1024$  pixels. Our objective is to perform pairwise comparisons of all images within this subset to determine whether two images originate from the same camera, a total of 8385 comparisons. This type of large-scale comparison exercise aligns with practical applications in industry. By maintaining a controlled and uniform image size, the approach focuses on accurately identifying images from the same source among a large collection of images.

The DWT-based extraction method of [29, 11] was performed using code from <https://github.com/polimi-ispl/prnu-python>, a Python implementation of the Binghampton Matlab PRNU library [15]; our proposed wavelet-domain algorithms were implemented using modifications to this code. The DTCWT-based PRNU extraction (in the original form of [45] as well as our proposed modifications to the technique), was implemented in Python based on Matlab code made available by the authors [44]. We opted to use our own Python implementation of [45] to ensure as fair a comparison as possible of runtimes between the methods.

In our comparison, we evaluated results using several key metrics: TPR and TNR based on the Youden index threshold (threshold 1 as described in Section 2.3), TPR when TNR is fixed at  $R = 0.99$  to minimize false identifications in real-world applications (threshold 2), area under the curve (AUC), and computational time in seconds, including extraction time per pair of images, comparison time per pair of images, and the total time for all comparisons. We compared four approaches to DWT-based extraction: the original LAW method, the grayscale first WDLAW method (gray-WDLAW), the wavelet domain grayscale approach (WDLAW-gray), and the full RGB-channel wavelet domain fingerprint (rgb-WDLAW). Additionally, we considered four methods based on the DTCWT: the original method of [45], as well as this DTCWT-based algorithm including additional image domain artifact removal (zero mean filtering, Fourier domain Wiener filtering) as described in Section 2.2.1; we compared these methods with the hybrid-LAW version of DTCWT extraction

(LAW-DTCWT) and our proposed gray-WDLAW-DTCWT method introduced in Section 3.3. Our goal was to identify methods that achieve both high accuracy and efficient computation.

To ensure a fair comparison, as far as possible all parameters involved in the estimation and computation of LAW-related methods were kept consistent, including the choice of wavelet, decomposition level, and noise variance. The recommended settings from the LAW method were applied, specifically using the Daubechies-4 (db4) wavelet and a primary decomposition level of  $J = 4$ . We set the noise variance to be  $\sigma_n = 1.8^2$ , following previous studies [45].

## 4.2. Experimental results

### 4.2.1. DWT-based extraction

The results shown in Tables 1 and 2 demonstrate that, overall, our WDLAW methods outperform the original LAW method, either by maintaining similar accuracy with improved speed or by achieving higher TPR and TNR across all thresholds, along with a larger AUC. Specifically, the gray-WDLAW method outperforms the LAW method across all measures of accuracy. This improvement indicates a significantly enhanced ability to accurately identify images originating from the same source.

Table 1: Comparison of image source identification accuracy using DWT-based methods on the dataset.

Method	TPR/TNR (Youden)	TPR@TNR=0.99	AUC
LAW	0.87/0.95	0.80	0.95
gray-WDLAW	0.90/0.97	0.87	0.96
rgb-WDLAW	0.88/0.98	0.84	0.96
WDLAW-gray	0.89/0.98	0.85	0.96

When considering computation time, our proposed gray-WDLAW method outperforms the original LAW method on this dataset. The average comparison time of the proposed method is noticeably faster than LAW primarily because we retain the fingerprints in the wavelet domain, which significantly reduces the number of coefficients involved in the comparison (see Section 3.1).

Table 2: Computation time (in seconds) using DWT-based methods: average fingerprint extraction time (per pair), comparison time (per pair), and total runtime.

Method	Extraction	Comparison	Total Time
LAW	1.127	0.010	96.700
gray-WDLAW	0.502	0.001	37.779
rgb-WDLAW	1.251	0.004	90.353
WDLAW-gray	1.207	0.004	86.079

A drawback is, however, observed with the rgb-WDLAW method, which exhibits the longest fingerprint extraction time. On larger datasets, this limitation could lead to substantially increased computation times. From an application perspective, although rgb-WDLAW yields high TNR and accuracy, it also increases storage requirements for the extracted fingerprints due to the three DWT computations (one for each channel). The trade-off between computation time, storage cost, and accuracy gains may not always justify its use in practical scenarios. The wavelet domain grayscaling method performs similarly to the full RGB fingerprint extraction, indicating that the additional information provided by the multichannel DWT does not bring significant benefits; we suggest that its decreased computational cost and substantially improved accuracy and subsequent the ability to identify images from the same source, makes our proposed gray-WDLAW technique a practical and realistic option for real-world company applications.

#### 4.2.2. DTCWT-based extraction

The results presented in Table 3 and Table 4 correspond to the methods utilising the DTCWT. Concerning the residual image denoising method of [45], we observe poor results in terms of accuracy, whether we include artifact removal or not when compared to the DWT-based results in Table 1. We note here, however, that this approach was developed for the tampering localisation application in [45] and not fingerprint comparison specifically. Both the hybrid LAW-DTCWT and our proposed gray-WDLAW-DTCWT methods achieve high accuracy, comparable to the wavelet domain DWT-based extraction methods (see Table 3).

Table 3: Comparison of image source identification accuracy using DTCWT-based methods on the dataset.

Method	TPR/TNR (Youden)	TPR@TNR=0.99	AUC
DTCWT	0.44/0.84	0.08	0.58
DTCWT with artifact removal	0.30/0.83	0.06	0.55
LAW-DTCWT	0.88/0.98	0.85	0.95
gray-WDLAW-DTCWT	0.90/0.96	0.85	0.97

As observed in [45], the DTCWT-based methods have higher extraction times than the DWT-based methods, see Table 4. This is to be expected due to the increased directional wavelet filtering (computation of the six subimages) of the DTCWT. Our wavelet domain approach, gray-WDLAW-DTCWT, has similar performance to the hybrid approach, but is significantly faster in extraction time, sacrificing a little on the comparison time.

## 5. Discussion and Conclusion

This study introduces a *wavelet-domain* locally adaptive window-based denoising method that builds upon previous SPN extraction techniques. Our

Table 4: Computation time (in seconds) using DTCWT-based methods: average fingerprint extraction time (per pair), comparison time (per pair), and total runtime.

Method	Extraction	Comparison	Total Time
DTCWT	2.775	0.001	371.310
DTCWT with artifact removal	3.248	0.001	434.180
LAW-DTCWT	2.773	0.001	372.960
gray-WDLAW-DTCWT	1.543	0.004	233.960

approach simplifies existing methodology by removing redundant steps that could degrade fingerprint detection accuracy and introduce unnecessary computational cost when performing SPN comparisons. In practical applications, where security agencies may need to identify cameras from vast collections of images, the computational cost of wavelet inversion can contribute significantly to computation. By eliminating the need for the inversion, our proposed gray-WDLAW technique offers a more efficient solution, reducing processing time while maintaining the integrity of the fingerprinting process. Experimental evaluations demonstrate that our method is both faster and more accurate in identifying camera sensor fingerprints. Further comparisons show that the proposed method is versatile, working effectively not only with the DWT but also with other more recent wavelet decomposition techniques such as the DTCWT. Our work demonstrates that, depending on the application or researchers' needs, performance and/or efficiency improvements can be gained by adopting our general approach.

Future work could explore alternative similarity metrics beyond cosine similarity, which was chosen for its simplicity and computational efficiency. Binary Hamming distance may serve as an efficient alternative for similarity testing, particularly for data storage or compression purposes [8]. In addition, we suggest that wavelet domain approaches may be able to be combined with other strategies for efficient storage and comparison of PRNU fingerprints, such as those introduced in [2, Section VII]. Beyond Mihcak's filters, other filtering techniques [5, 4, 14] could also be integrated into the WDLAW framework: since our focus is on structural modifications rather than specific filtering methods, users are free to explore and incorporate any filter that fits within this structure.

## Acknowledgments

The work in this article stemmed from initial insights gained at the ITT19 interdisciplinary workshop run by the EPSRC Centre for Doctoral Training in Statistical Applied Mathematics at Bath (SAMBa), grant number EP/S022945/1. We would in particular like to thank Kamran Arora from the University of Bath for helpful discussions during the workshop.

## References

- [1] Akshatha, K., Karunakar, A.K., Anitha, H., Raghavendra, U., Shetty, D., 2016. Digital camera identification using prnu: A feature based approach. *Digital Investigation* 19, 69–77.
- [2] Al-Ani, M., Khelifi, F., 2016. On the SPN estimation in image forensics: A systematic empirical evaluation. *IEEE Transactions on Information Forensics and Security* 12, 1067–1081.
- [3] Albisani, C., Iuliani, M., Piva, A., 2021. Checking PRNU usability on modern devices, in: *ICASSP 2021-2021 IEEE International Conference on Acoustics, Speech and Signal Processing (ICASSP)*, IEEE. pp. 2535–2539.
- [4] Amerini, I., Caldelli, R., Cappellini, V., Picchioni, F., Piva, A., 2009. Analysis of denoising filters for photo response non uniformity noise extraction in source camera identification, in: *2009 16th International Conference on Digital Signal Processing*, IEEE. pp. 1–7.
- [5] Argenti, F., Torricelli, G., Alparone, L., 2006. MMSE filtering of generalised signal-dependent noise in spatial and shift-invariant wavelet domains. *Signal Processing* 86, 2056–2066.
- [6] Bartlow, N., Kalka, N., Cukic, B., Ross, A., 2009. Identifying sensors from fingerprint images, in: *2009 IEEE Computer Society Conference on Computer Vision and Pattern Recognition Workshops*, IEEE. pp. 78–84.
- [7] Bayram, S., Sencar, H., Memon, N., Avcibas, I., 2005. Source camera identification based on CFA interpolation, in: *IEEE International Conference on Image Processing 2005*, IEEE. pp. III–69.
- [8] Bayram, S., Sencar, H.T., Memon, N., 2012. Efficient sensor fingerprint matching through fingerprint binarization. *IEEE Transactions on Information Forensics and Security* 7, 1404–1413.
- [9] Cao, H., Kot, A.C., 2009. Accurate detection of demosaicing regularity for digital image forensics. *IEEE Transactions on Information Forensics and Security* 4, 899–910.
- [10] Chen, C., Stamm, M.C., 2015. Camera model identification framework using an ensemble of demosaicing features, in: *2015 IEEE International Workshop on Information Forensics and Security (WIFS)*, IEEE. pp. 1–6.
- [11] Chen, M., Fridrich, J., Goljan, M., Lukás, J., 2008. Determining image origin and integrity using sensor noise. *IEEE Transactions on Information Forensics and Security* 3, 74–90.
- [12] Choi, K.S., Lam, E.Y., Wong, K.K., 2006. Automatic source camera identification using the intrinsic lens radial distortion. *Optics Express* 14, 11551–11565.

- [13] Chui, C.K., 1992. An Introduction to Wavelets. volume 1. Academic Press.
- [14] Cortiana, A., Conotter, V., Boato, G., De Natale, F.G., 2011. Performance comparison of denoising filters for source camera identification, in: Media Watermarking, Security, and Forensics III, SPIE. pp. 60–65.
- [15] Digital Data Embedding Laboratory, Binghamton University, . Camera fingerprint - matlab implementation. URL: [https://dde.binghamton.edu/download/camera\\\_fingerprint/](https://dde.binghamton.edu/download/camera\_fingerprint/).
- [16] Freire-Obregon, D., Narducci, F., Barra, S., Castrillon-Santana, M., 2019. Deep learning for source camera identification on mobile devices. Pattern Recognition Letters 126, 86–91.
- [17] Garfinkel, S.L., 2010. Digital forensics research: The next 10 years. Digital Investigation 7, S64–S73.
- [18] Gisolf, F., Malgoezar, A., Baar, T., Geradts, Z., 2013. Improving source camera identification using a simplified total variation based noise removal algorithm. Digital Investigation 10, 207–214.
- [19] Gloe, T., Böhme, R., 2010. The 'Dresden Image Database' for benchmarking digital image forensics, in: Proceedings of the 2010 ACM Symposium on Applied Computing, pp. 1584–1590.
- [20] Gloe, T., Pfennig, S., Kirchner, M., 2012. Unexpected artefacts in PRNU-based camera identification: a 'dresden image database' case-study, in: Proceedings of the ACM Conference on Multimedia and Security, pp. 109–114.
- [21] Goljan, M., Fridrich, J., 2008. Camera identification from cropped and scaled images, in: Security, Forensics, Steganography, and Watermarking of Multimedia Contents X, SPIE. pp. 154–166.
- [22] Goljan, M., Fridrich, J., Filler, T., 2009. Large scale test of sensor fingerprint camera identification, in: Media Forensics and Security, SPIE. pp. 170–181.
- [23] Huang, N., He, J., Zhu, N., Xuan, X., Liu, G., Chang, C., 2018. Identification of the source camera of images based on convolutional neural network. Digital Investigation 26, 72–80.
- [24] Júnior, P.R.M., Bondi, L., Bestagini, P., Rocha, A., Tubaro, S., 2019. A prnu-based method to expose video device compositions in open-set setups, in: 2019 IEEE International Conference on Image Processing (ICIP), IEEE. pp. 96–100.
- [25] Kang, X., Li, Y., Qu, Z., Huang, J., 2011. Enhancing source camera identification performance with a camera reference phase sensor pattern noise. IEEE Transactions on Information Forensics and Security 7, 393–402.

- [26] Kharrazi, M., Sencar, H.T., Memon, N., 2004. Blind source camera identification, in: 2004 International Conference on Image Processing, 2004. ICIP'04., IEEE. pp. 709–712.
- [27] Kingsbury, N., 1998. The dual-tree complex wavelet transform: a new efficient tool for image restoration and enhancement, in: 9th European Signal Processing Conference (EUSIPCO 1998), IEEE. pp. 1–4.
- [28] Kirchner, M., Gloe, T., 2015. Forensic camera model identification. Handbook of Digital Forensics of Multimedia Data and Devices , 329–374.
- [29] Lukas, J., Fridrich, J., Goljan, M., 2006. Digital camera identification from sensor pattern noise. IEEE Transactions on Information Forensics and Security 1, 205–214.
- [30] Mandelli, S., Cozzolino, D., Bestagini, P., Verdoliva, L., Tubaro, S., 2020. Cnn-based fast source device identification. IEEE Signal Processing Letters 27, 1285–1289.
- [31] Manisha, Li, C.T., Lin, X., Kotegar, K.A., 2022. Beyond prnu: Learning robust device-specific fingerprint for source camera identification. Sensors 22, 7871.
- [32] Mihcak, M.K., Kozintsev, I., Ramchandran, K., 1999a. Spatially adaptive statistical modeling of wavelet image coefficients and its application to denoising, in: 1999 IEEE International Conference on Acoustics, Speech, and Signal Processing. Proceedings. ICASSP99 (Cat. No. 99CH36258), IEEE. pp. 3253–3256.
- [33] Mihcak, M.K., Kozintsev, I., Ramchandran, K., Moulin, P., 1999b. Low-complexity image denoising based on statistical modeling of wavelet coefficients. IEEE Signal Processing Letters 6, 300–303.
- [34] Nason, G.P., 2008. Wavelet Methods in Statistics with R. Springer.
- [35] Neelamani, R., Choi, H., Baraniuk, R., 2004. ForWaRD: Fourier-wavelet regularized deconvolution for ill-conditioned systems. IEEE Transactions on Signal Processing 52, 418–433.
- [36] Redi, J.A., Taktak, W., Dugelay, J.L., 2011. Digital image forensics: A booklet for beginners. Multimedia Tools and Applications 51, 133–162.
- [37] Rocha, A., Scheirer, W., Boulton, T., Goldenstein, S., 2011. Vision of the unseen: Current trends and challenges in digital image and video forensics. ACM Computing Surveys (CSUR) 43, 1–42.
- [38] Selesnick, I.W., Baraniuk, R.G., Kingsbury, N.C., 2005. The dual-tree complex wavelet transform. IEEE Signal Processing Magazine 22, 123–151.

- [39] Sundararajan, D., 2016. Discrete wavelet transform: a signal processing approach. John Wiley & Sons.
- [40] Van, L.T., Emmanuel, S., Kankanhalli, M.S., 2007. Identifying source cell phone using chromatic aberration, in: 2007 IEEE International Conference on Multimedia and Expo, IEEE. pp. 883–886.
- [41] Vidakovic, B., 2009. Statistical Modeling by Wavelets. John Wiley & Sons.
- [42] Wang, B., Yin, J., Tan, S., Li, Y., Li, M., 2018. Source camera model identification based on convolutional neural networks with local binary patterns coding. Signal Processing: Image Communication 68, 162–168.
- [43] Youden, W.J., 1950. Index for rating diagnostic tests. Cancer 3, 32–35.
- [44] Zeng, H., . Source camera identification with dual-tree complex wavelet transform: Matlab codes. URL: [https://github.com/zengh5/SCI\\\_DTCWT](https://github.com/zengh5/SCI\_DTCWT).
- [45] Zeng, H., Wan, Y., Deng, K., Peng, A., 2020. Source camera identification with dual-tree complex wavelet transform. IEEE Access 8, 18874–18883.